Modeling Impact of Moving Scatterers on Doppler Spectrum in Wideband Vehicle-to-Vehicle Channels

Alenka Zajić
School of Electrical and Computer Engineering
Georgia Institute of Technology, Atlanta, GA 30332 USA

***Abstract*— A three-dimensional (3-D) geometrical propagation model that includes both stationary and moving scatterers around the transmitter and receiver for *wideband* vehicle-to-vehicle (V-to-V) communications is proposed. Based on the geometrical model, a 3-D reference model for wideband multiple-input multiple-output (MIMO) V-to-V multipath fading channels is developed. From the reference model, the corresponding space-Doppler power spectral density is derived. Finally, the theoretical results are compared with measured data in urban environment, the model with only stationary scatterers, and the narrowband channel model with moving and stationary scatterers. The results show the best agreement between the measured and the modelled wideband channel model with stationary and moving scatterers.**

I. Introduction

Vehicle-to-vehicle (V-to-V) communication systems have recently drawn great attention, because they have the potential to improve convenience and safety of automobile transportation. The simulation and performance evaluation of V-to-V systems, as well as the design of future, improved systems, requires a deep understanding of the underlying propagation channels.

Vehicle-to-vehicle (V-to-V) channels have characteristics that are significantly different from the better-explored fixed-to-mobile (F-to-M) cellular channels [1]. In V-to-V channels, both the transmitter ($\mathrm{T_x}$) and the receiver ($\mathrm{R_x}$) are in motion, equipped with low elevation antennas, and surrounded by local scatterers. Furthermore, the channel characteristics of V-to-V channels are influenced by the properties of the environment around the communicating vehicles and by typical traffic patterns. Many V-to-V channel models have been proposed in the literature and are summarized in [2], [3]. However, most of these models do not take into account mobility of scatterers. The mobility of scatterers may significantly impact Doppler spectrum, so it is important to correctly account for that effect.

The impact of moving scatterers on Doppler spectrum in F-to-M cellular and fixed-to-fixed (F-to-F) channels has been studied in [4]-[8]. More recently, modeling of V-to-V channels in the presence of moving scatterers has been discussed in [9]-[11]. However, none of these models takes into account that the rays in V-to-V channels can be both double-bounced and single-bounced [12]. Furthermore, these models assume that the field incident on the $\mathrm{T_x}$ or the $\mathrm{R_x}$ antenna is composed of a number of waves travelling only in the horizontal plane. However, measurements show that this assumption does not seem appropriate for an urban environment where the $\mathrm{T_x}$ and $\mathrm{R_x}$ antenna arrays are often located in close proximity to and lower than surrounding buildings [12]. To overcome these shortcomings, in [13], we have proposed a three-dimensional (3-D) narrow-band reference channel model that includes both stationary and moving scatterers around the $\mathrm{T_x}$ and the $\mathrm{R_x}$. In this paper, we extend this work to wideband channels.

To describe the proposed wideband model, the geometrical concentric-cylinder model for wideband V-to-V channels [12] is extended to include the moving scatterers. Then, a parametric reference model that employs the new 3-D geometrical model and constructs the channel impulse response as a combination of line-of-sight (LoS), single-bounced at the transmitter (SBT), single-bounced at the receiver (SBR), and double-bounced (DB) rays is proposed. From the new reference model, the corresponding space-Doppler power spectral density for a 3-D non-isotropic scattering environment is derived. To illustrate validity and need for the proposed model, we compare the modeled wideband Doppler spectrum with stationary and moving scatterers with the measured Doppler spectrum obtained from the measurement campaign described in [12], the modelled narrowband Doppler spectrum with stationary and moving scatterers [13], and the modelled Doppler spectrum with only stationary scatterers [14]. The results show the best agreement between the measured Doppler spectrum and the modelled wideband channel Doppler spectrum with stationary and moving scatterers.

The remainder of the paper is organized as follows. Section II describes the geometrical model and presents a 3-D reference model for wideband MIMO V-to-V channels with stationary and moving scatterers. Section III derives the sD-psd for a 3-D non-isotropic scattering environment. Section IV compares the theoretical results with measured data in urban environment. Finally, Section V provides some concluding remarks.

II. A Reference Model for Wideband V-to-V Channels with Stationary and Moving Scatterers

This paper considers a wideband communication link with L_T transmit and L_R receive omnidirectional antenna elements. Both the transmitter ($\mathrm{T_x}$) and receiver ($\mathrm{R_x}$) are in motion and are equipped with low elevation antennas. The radio propagation environment is characterized by 3-D stationary and moving scattering with either line-of-sight (LoS) or non-line-of-sight (NLoS) conditions between the $\mathrm{T_x}$ and the $\mathrm{R_x}$.

Fig. 1 shows the concentric-cylinders model with moving and stationary scatterers. The concentric-cylinders model defines four vertical cylinders, two around the $\mathrm{T_x}$ and another two around the $\mathrm{R_x}$. Around the transmitter, M_S fixed omnidirectional scatterers occupy a volume between cylinders of radii R_{t1} and R_{t2}, while M_M moving omnidirectional scatterers occupy the area between circles of radii R_{t1} and R_{t2}. It is assumed that the M_S scatterers lie on L cylindric surfaces, while M_M scatterers lie on L concentric circles of radii $R_{t1} \leq R_t^{(l)} \leq R_{t2}$, where $1 \leq l \leq L$. The l^{th} surface contains $M_S^{(l)}$ fixed and $M_M^{(l)}$ omnidirectional scatterers. The $(m,l)^{th}$ stationary transmit scatterer is denoted by $S_T^{(m,l)}$ where $1 \leq m \leq M_S^{(l)}$, while the $(f,l)^{th}$ moving scatterer is denoted by $S_{TM}^{(f,l)}$, where $1 \leq f \leq M_M^{(l)}$. Similarly, around the receiver, N_S fixed omnidirectional scatterers occupy a volume between cylinders of radii R_{r1} and R_{r2}, while N_M moving omnidirectional scatterers occupy the area between circles of radii R_{r1} and R_{r2}. It is assumed that the N_S scatterers lie on K cylindric surfaces of radii $R_{r1} \leq R_r^{(k)} \leq R_{r2}$, while N_M scatterers lie on K concentric circles of radii $R_{r1} \leq R_r^{(k)} \leq R_{r2}$, where $1 \leq k \leq K$. The k^{th} cylindric surface contains $N_S^{(k)}$ fixed and $N_M^{(k)}$ omnidirectional scatterers. The $(n,k)^{th}$ stationary receive scatterer is denoted by $S_R^{(n,k)}$, where $1 \leq n \leq N_S^{(k)}$, while the $(w,k)^{th}$ moving scatterer is denoted by $S_{RM}^{(w,k)}$ where $1 \leq w \leq N_M^{(k)}$.

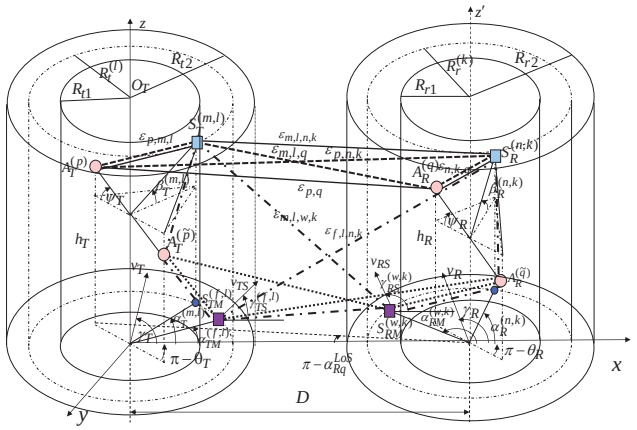

Fig. 1. The concentric-cylinder model with LoS, SBT, SBR, and DB rays for moving and stationary scatterers in wideband MIMO V-to-V channels with $L_t = L_r = 2$ antenna elements.

The distance between the centers of the $\mathrm{T_x}$ and $\mathrm{R_x}$ cylinders is D. It is assumed that the radii R_{t2} and R_{r2} are sufficiently smaller than the distance D (local scattering condition). Furthermore, it is assumed that the distance D is smaller than $4R_{t1}R_{r1}L_r/(\lambda(L_t-1)(L_r-1))$ (channel does not experience keyhole behavior [15]), where λ denotes the carrier wavelength. The spacing between antenna elements at the $\mathrm{T_x}$ and $\mathrm{R_x}$ is denoted by d_T and d_R, respectively. It is assumed that d_T and d_R are much smaller than the radii R_{t1} and R_{r1}.

The distance $\epsilon_{p,m,l}$ is the distance between the p^{th} antenna $A_T^{(p)}$ and the $(m,l)^{\text{th}}$ stationary scatterer placed around the $\mathrm{T_x}$, i.e., $A_T^{(p)} - S_T^{(m,l)}$. Similarly, symbols $\epsilon_{m,l,q}$, $\epsilon_{p,n,k}$, $\epsilon_{n,k,q}$, $\epsilon_{m,l,n,k}$, $\epsilon_{p,f,l}$, $\epsilon_{f,l,q}$, $\epsilon_{p,w,k}$, $\epsilon_{w,k,q}$, $\epsilon_{f,l,w,k}$, $\epsilon_{m,l,w,k}$, $\epsilon_{f,l,n,k}$, and ϵ_{pq} denote distances $S_T^{(m,l)}$ - $A_R^{(q)}$, $A_T^{(p)}$ - $S_R^{(n,k)}$, $S_R^{(n,k)}$ - $A_R^{(q)}$, $S_T^{(m,l)}$ - $S_R^{(n,k)}$, $A_T^{(p)}$ - $S_{TM}^{(f,l)}$, $S_{TM}^{(f,l)}$ – $A_R^{(q)}$, $A_T^{(p)}$ - $S_{RM}^{(w,k)}$, $S_{RM}^{(w,k)}$ – $A_R^{(q)}$, $S_{TM}^{(f,l)}$ - $S_{RM}^{(w,k)}$, $S_T^{(m,l)}$ - $S_{RM}^{(w,k)}$, $S_{TM}^{(f,l)}$ - $S_R^{(n,k)}$, and $A_T^{(p)}$ - $A_R^{(q)}$ respectively, as shown in Fig. 1.

The $\mathrm{T_x}$ and $\mathrm{R_x}$ antenna heights are denoted h_T and h_R, respectively, angles θ_T and θ_R in Fig. 1 describe the orientation of the $\mathrm{T_x}$ and $\mathrm{R_x}$ antenna array in the x - y plane, respectively, and angles ψ_T and ψ_R describe the elevation of the $\mathrm{T_x}$'s antenna array and the $\mathrm{R_x}$'s antenna array relative to the x - y plane, respectively. The $\mathrm{T_x}$ and $\mathrm{R_x}$ are moving with speeds v_T and v_R in directions described by angles γ_T and γ_R in the x-y plane (relative to the x-axis), respectively. The moving scatterers around the $\mathrm{T_x}$ and $\mathrm{R_x}$ are moving with relative speeds v_{TS} and v_{RS} with respect to the velocities of the $\mathrm{T_x}$ and $\mathrm{R_x}$, respectively, and in the directions described by angles $\gamma_{TS}^{(f,l)}$ and $\gamma_{RS}^{(w,k)}$ in the x-y plane (relative to the x-axis), respectively.

Symbol $\alpha_T^{(m,l)}$ represents the azimuth angle of departure (AAoD) of the wave that impinges on the *stationary* scatterer $S_T^{(m,l)}$, while $\alpha_R^{(n,k)}$ is the azimuth angle of arrival (AAoA) of the wave scattered from the stationary scatterer $S_R^{(n,k)}$. Similarly, the symbols $\beta_T^{(m,l)}$ and $\beta_R^{(n,k)}$ denote the elevation angle of departure (EAoD) and the elevation angle of arrival (EAoA) of the waves that interact with stationary scatterers around the $\mathrm{T_x}$ and $\mathrm{R_x}$, respectively. On the other hand, symbols $\alpha_{TM}^{(f,l)}$ and $\alpha_{RM}^{(w,k)}$ represent the angle of departure (AoD) and the angle of arrival (AoA) of the waves that interact with the *moving* scatterers around the $\mathrm{T_x}$ and $\mathrm{R_x}$, respectively. Finally, symbols α_{Tp}^{LoS} and α_{Rq}^{LoS} denote the AAoDs and AAoAs of the LoS paths.

We can observe from the 3-D geometrical model in Fig. 1 that some waves from the $\mathrm{T_x}$ antenna elements may traverse directly to the $\mathrm{R_x}$ antenna elements (LoS rays), while others are single-bounced at the $\mathrm{T_x}$ (SBT), single-bounced at the $\mathrm{R_x}$ (SBR), and/or double-bounced (DB). Therefore, the complex faded envelope of the link $A_T^{(p)}$ - $A_R^{(q)}$ can be written as

$$\begin{aligned} h_{pq}(t,\tau) &= h_{pq}^{LoS}(t,\tau) + h_{pq}^{SBT}(t,\tau) \\ &+ h_{pq}^{SBR}(t,\tau) + h_{pq}^{DB}(t,\tau), \end{aligned} \tag{1}$$

where the the respective components are

$$h_{pq}^{LoS}(t,\tau) = \sqrt{\frac{\Omega_{pq}K}{K+1}} e^{\left(j2\pi f_{pq}^{LoS} t - j\frac{2\pi}{\lambda}\epsilon_{pq}\right)} \delta(\tau - \tau_{pq}), \tag{2}$$

$$h_{pq}^{SBT}(t,\tau) = \frac{\lambda}{4\pi\sqrt{D^{\gamma}(K+1)}} \Bigg[\lim_{M_S\to\infty} \sum_{l=1}^{L} \sqrt{\frac{\eta_{T_S}}{M_S^{(l)}}} \sum_{m=1}^{M_S^{(l)}}$$

$$(1 - \frac{\gamma}{2}\frac{R_t^{(l)}}{D}) e^{\left(j2\pi f_{ml}^{SBT} t - j\frac{2\pi}{\lambda}(\epsilon_{p,m,l} + \epsilon_{m,l,q}) + j\phi_{pq,ml}^{SBT}\right)}$$

$$\delta(\tau - \tau_{m,l}) + \lim_{M_M\to\infty} \sum_{l=1}^{L} \sqrt{\frac{\eta_{T_M}}{M_M^{(l)}}} \sum_{f=1}^{M_M^{(l)}} (1 - \frac{\gamma}{2}\frac{R_t^{(l)}}{D})$$

$$e^{\left(j2\pi f_{fl}^{SBT}t - j\frac{2\pi}{\lambda}(\epsilon_{p,f,l}+\epsilon_{f,l,q}) + j\phi_{pq,fl}^{SBT}\right)}\delta(\tau-\tau_{f,l})\Bigg], \quad (3)$$

$$h_{pq}^{SBR}(t,\tau) = \frac{\lambda}{4\pi\sqrt{D^{\gamma}(K+1)}}\Bigg[\lim_{N_S\to\infty}\sum_{k=1}^{K}\sqrt{\frac{\eta_{R_S}}{N_S^{(k)}}}\sum_{n=1}^{N_S^{(k)}}$$

$$(1-\frac{\gamma}{2}\frac{R_r^{(k)}}{D})e^{(j2\pi f_{nk}^{SBR}t - j\frac{2\pi}{\lambda}(\epsilon_{p,n,k}+\epsilon_{n,k,q}) + j\phi_{pq,nk}^{SBR})}$$

$$\delta(\tau-\tau_{n,k}) + \lim_{N_M\to\infty}\sum_{k=1}^{K}\sqrt{\frac{\eta_{R_M}}{N_M^{(k)}}}\sum_{w=1}^{M_M^{(k)}}(1-\frac{\gamma}{2}\frac{R_r^{(k)}}{D})$$

$$e^{(j2\pi f_{wk}^{SBR}t - j\frac{2\pi}{\lambda}(\epsilon_{p,w,k}+\epsilon_{w,k,q}) + j\phi_{pq,wk}^{SBR})}\delta(\tau-\tau_{w,k})\Bigg], \quad (4)$$

$$h_{pq}^{DB}(t,\tau) = \frac{\lambda}{4\pi\sqrt{D^{\gamma}(K+1)}}\Bigg[\lim_{M_S,N_S\to\infty}\sum_{l=1}^{L}\sum_{m=1}^{M_S^{(l)}}\sum_{k=1}^{K}\sum_{n=1}^{N_S^{(k)}}$$

$$\sqrt{\frac{\eta_{TR_1}}{M_S^{(l)}N_S^{(k)}}}(1-\frac{\gamma}{2}\frac{R_t^{(l)}+R_r^{(k)}}{2D})\delta(\tau-\tau_{m,l,n,k})$$

$$e^{(j2\pi f_{mlnk}^{DB}t - j\frac{2\pi}{\lambda}(\epsilon_{p,m,l}+\epsilon_{m,l,n,k}+\epsilon_{n,k,q}) + j\phi_{pq,mlnk}^{DB})} + \lim_{M_M,N_S\to\infty}$$

$$\sum_{l=1}^{L}\sum_{f=1}^{M_M^{(l)}}\sum_{k=1}^{K}\sum_{n=1}^{N_S^{(k)}}\sqrt{\frac{\eta_{TR_2}}{M_M^{(l)}N_S^{(k)}}}(1-\frac{\gamma}{2}\frac{R_t^{(l)}+R_r^{(k)}}{2D})$$

$$e^{(j2\pi f_{flnk}^{DB}t - j\frac{2\pi}{\lambda}(\epsilon_{p,f,l}+\epsilon_{f,l,n,k}+\epsilon_{n,k,q}) + j\phi_{pq,flnk}^{DB})}\delta(\tau-\tau_{f,l,n,k})$$

$$+\lim_{M_S,N_M\to\infty}\sum_{l=1}^{L}\sum_{m=1}^{M_S^{(l)}}\sum_{k=1}^{K}\sum_{w=1}^{N_M^{(k)}}\sqrt{\frac{\eta_{TR_3}}{M_S^{(l)}N_M^{(k)}}}(1-\frac{\gamma}{2}\frac{R_t^{(l)}+R_r^{(k)}}{2D})$$

$$e^{j2\pi f_{mlwk}^{DB}t - j\frac{2\pi}{\lambda}(\epsilon_{p,m,l}+\epsilon_{m,l,w,k}+\epsilon_{w,k,q}) + j\phi_{pq,mlwk}^{DB}}\delta(\tau-\tau_{m,l,w,k})$$

$$+\lim_{M_M,N_M\to\infty}\sum_{l=1}^{L}\sum_{f=1}^{M_M^{(l)}}\sum_{k=1}^{K}\sum_{w=1}^{N_M^{(k)}}\sqrt{\frac{\eta_{TR_4}}{M_M^{(l)}N_M^{(k)}}}(1-\frac{\gamma}{2}\frac{R_t^{(l)}+R_r^{(k)}}{2D})$$

$$e^{j2\pi f_{flwk}^{DB}t - j\frac{2\pi}{\lambda}(\epsilon_{p,f,l}+\epsilon_{f,l,w,k}+\epsilon_{w,k,q}) + j\phi_{pq,flwk}^{DB}}\delta(\tau-\tau_{f,l,w,k})\Bigg] \quad (5)$$

where K describes how the total signal power is split between the LoS and NLoS components, γ denotes pathloss exponent, $p \in \{1,\ldots,L_t\}$ and $q \in \{1,\ldots,L_r\}$. Here we assume that the relative power allocated to the SBT, SBR, and DB components is respectively $\eta_T = \eta_{T_S} + \eta_{T_M}$, $\eta_R = \eta_{R_S} + \eta_{R_M}$, and $\eta_{TR} = \eta_{TR_1} + \eta_{TR_2} + \eta_{TR_3} + \eta_{TR_4}$ such that $\eta_T + \eta_R + \eta_{TR} = 1$. These parameters have to be either set during simulations or estimated from measurements. The Doppler shift frequencies in this model can be calculated as follows:

$$f_{pq}^{LoS} = f_{\mathrm{Rmax}}\cos(\alpha_{Rq}^{LoS}-\gamma_R) - f_{\mathrm{Tmax}}\cos(\alpha_{Rq}^{LoS}+\gamma_T) \quad (6)$$

$$f_{ml}^{SBT} = f_{\mathrm{Tmax}}\cos(\alpha_T^{(m,l)}-\gamma_T)\cos\beta_T^{(m,l)} + f_{\mathrm{Rmax}}(\Delta_T^{(l)}$$
$$\sin\gamma_R\sin\alpha_T^{(m,l)} - \cos\gamma_R), \quad (7)$$

$$f_{fl}^{SBT} = f_{\mathrm{Tmax}}\cos(\alpha_{TM}^{(f,l)}-\gamma_T) + f_{\mathrm{Rmax}}(\Delta_T^{(l)}\sin\gamma_R$$
$$\sin\alpha_{TM}^{(f,l)} - \cos\gamma_R) - f_{\mathrm{TSmax}}[\cos(\alpha_{TM}^{(f,l)}-\gamma_{TS}^{(f,l)})$$
$$+\Delta_T^{(l)}\sin\gamma_R\sin\alpha_{TM}^{(f,l)} - \cos\gamma_{TS}^{(f,l)}], \quad (8)$$

$$f_{nk}^{SBR} = f_{\mathrm{Tmax}}(\Delta_R^{(k)}\sin\gamma_T\sin\alpha_R^{(n,k)} + \cos\gamma_T)$$
$$+f_{\mathrm{Rmax}}\cos(\alpha_R^{(n,k)}-\gamma_R)\cos\beta_R^{(n,k)}, \quad (9)$$

$$f_{wk}^{SBR} = f_{\mathrm{Tmax}}(\Delta_R^{(k)}\sin\gamma_T\sin\alpha_{RM}^{(w,k)} + \cos\gamma_T)$$
$$+f_{\mathrm{Rmax}}(\alpha_{RM}^{(w,k)}-\cos\gamma_R) - f_{\mathrm{RSmax}}[\cos(\alpha_{RM}^{(w,k)}-\gamma_{RS}^{(w,k)})$$
$$+\Delta_R^{(k)}\sin\gamma_T\sin\alpha_{RM}^{(w,k)} + \cos\gamma_{RS}^{(w,k)}], \quad (10)$$

$$f_{mlnk}^{DB} = f_{\mathrm{Tmax}}\cos(\alpha_T^{(m,l)}-\gamma_T)\cos\beta_T^{(m,l)}$$
$$+f_{\mathrm{Rmax}}\cos(\alpha_R^{(n,k)}-\gamma_R)\cos\beta_R^{(n,k)}, \quad (11)$$

$$f_{flnk}^{DB} = f_{\mathrm{Tmax}}\cos(\alpha_{TM}^{(f,l)}-\gamma_T) - f_{\mathrm{TSmax}}[\cos(\alpha_{TM}^{(f,l)}-\gamma_{TS}^{(f,l)})$$
$$-\cos\gamma_{TS}^{(f,l)}] + f_{\mathrm{Rmax}}\cos(\alpha_R^{(n,k)}-\gamma_R)\cos\beta_R^{(n,k)} \quad (12)$$

$$f_{mlwk}^{DB} = f_{\mathrm{Tmax}}\cos(\alpha_T^{(m,l)}-\gamma_T)\cos\beta_T^{(m,l)} - f_{\mathrm{RSmax}}[\cos($$
$$\alpha_{RM}^{(w,k)}-\gamma_{RS}^{(w,k)}) + \cos\gamma_{RS}^{(w,k)}] + f_{\mathrm{Rmax}}\cos(\alpha_{RM}^{(w,k)}-\gamma_R), \quad (13)$$

$$f_{flwk}^{DB} = f_{\mathrm{Tmax}}\cos(\alpha_{TM}^{(f,l)}-\gamma_T) + f_{\mathrm{Rmax}}\cos(\alpha_{RM}^{(w,k)}-\gamma_R)$$
$$-f_{\mathrm{TSmax}}[\cos(\alpha_{TM}^{(f,l)}-\gamma_{TS}^{(f,l)}) - \cos\gamma_{TS}^{(f,l)}]$$
$$-f_{\mathrm{RSmax}}[\cos(\alpha_{RM}^{(w,k)}-\gamma_{RS}^{(w,k)}) + \cos\gamma_{RS}^{(w,k)}], \quad (14)$$

where λ is the carrier wavelength, $\Delta_T^{(l)} = R_t^{(l)}/D$, $\Delta_R^{(k)} = R_r^{(k)}/D$, and frequencies $f_{\mathrm{Tmax}} = v_T/\lambda$, $f_{\mathrm{Rmax}} = v_R/\lambda$, $f_{\mathrm{TSmax}} = v_{TS}/\lambda$, and $f_{\mathrm{RSmax}} = v_{RS}/\lambda$ are the maximum Doppler frequencies associated with the $\mathrm{T_x}$, $\mathrm{R_x}$, the moving scatterers around the $\mathrm{T_x}$, and the moving scatterers around the $\mathrm{R_x}$, respectively. The direction of moving scatterers ($\gamma_{TS}^{(f,l)}$ and $\gamma_{RS}^{(w,k)}$), the AAoDs and AAoAs ($\alpha_T^{(m,l)}$ and $\alpha_R^{(n,k)}$), the EAoDs and EAoAs ($\beta_T^{(m,l)}$ and $\beta_R^{(n,k)}$), and the AoDs and AoAs ($\alpha_{TM}^{(f,l)}$ and $\alpha_{RM}^{(w,k)}$), are modeled as independent random variables. Several different scatterer distributions, such as uniform, Gaussian, Laplacian, and von Mises, are used in prior work to characterize the AAoDs, AAoAs, AoDs, and AoAs. We use the von Mises pdf because it approximates many of the previously mentioned distributions and admits closed-form solutions for many useful situations. The von Mises pdf is defined as $p(\theta) = \exp[\kappa\cos(\theta-\mu)]/2\pi I_0(\kappa)$ [16] where $\theta \in [-\pi,\pi)$, $I_0(\cdot)$ is the zeroth-order modified Bessel function of the first kind, $\mu \in [-\pi,\pi)$ is the mean angle at which the scatterers are distributed in the x–y plane, and κ controls the spread of scatterers around the mean. Similarly, prior work uses several different scatterer distributions, such as uniform, cosine, and Gaussian, to characterize the EAoAs and EAoDs. We use the pdf [17]

$$p(\varphi) = \begin{cases} \frac{\pi}{4|\varphi_m|}\cos\left(\frac{\pi}{2}\frac{\varphi}{\varphi_m}\right) & , \ |\varphi| \le |\varphi_m| \le \frac{\pi}{2} \\ 0 & , \ \text{otherwise} \end{cases} \quad (15)$$

where φ_m is the maximum elevation angle and lies in the range $0^\circ \le |\varphi_m| \le 20^\circ$. Finally, the radii $R_t^{(l)}$ and $R_r^{(k)}$ are characterized using the pdf $p(R) = 2R/(R_2^2 - R_1^2)$. This model also assumes that phases are uniformly distributed on the interval $[0, 2\pi)$ and independent from any other random variable.

From Fig. 1, the path lengths of the respective waves can be approximated as:

$$\epsilon_{m,l,n,k} \approx \epsilon_{f,l,w,k} \approx \epsilon_{m,l,w,k} \approx \epsilon_{f,l,n,k} \approx D,$$
$$\epsilon_{pq} \approx D - \frac{L_t+1-2p}{2}d_{Tx} + \frac{L_r+1-2q}{2}d_{Rx}, \quad (16)$$

$$\epsilon_{p,m,l} \approx R_t^{(l)} - \frac{L_t+1-2p}{2}\big[d_{Tx}\cos\alpha_T^{(m,l)}\cos\beta_T^{(m,l)} + d_{Ty}\sin\alpha_T^{(m,l)}\cos\beta_T^{(m,l)} + d_{Tz}\sin\beta_T^{(m,l)}\big] \quad (17)$$

$$\epsilon_{m,l,q} \approx D - \frac{L_r+1-2q}{2}d_R\cos\psi_R \times[\Delta_T^{(l)}\sin\theta_R\sin\alpha_T^{(m,l)} - \cos\theta_R], \quad (18)$$

$$\epsilon_{p,f,l} \approx R_t^{(l)} - \frac{L_t+1-2p}{2}d_T\cos(\theta_T - \alpha_{TM}^{(f,l)}) \quad (19)$$

$$\epsilon_{f,l,q} \approx D - \frac{L_r+1-2q}{2}d_R \times[\Delta_T^{(l)}\sin\theta_R\sin\alpha_{TM}^{(f,l)} - \cos\theta_R], \quad (20)$$

$$\epsilon_{p,n,k} \approx D - \frac{L_t+1-2p}{2}d_T\cos\psi_T \times[\Delta_R^{(k)}\sin\theta_T\sin\alpha_R^{(n,k)} + \cos\theta_T], \quad (21)$$

$$\epsilon_{n,k,q} \approx R_r^{(k)} - \frac{L_r+1-2q}{2}[d_{Rx}\cos\alpha_R^{(n,k)}\cos\beta_R^{(n,k)} + d_{Ry}\sin\alpha_R^{(n,k)}\cos\beta_R^{(n,k)} + d_{Rz}\sin\beta_R^{(n,k)}], \quad (22)$$

$$\epsilon_{p,w,k} \approx D - \frac{L_t+1-2p}{2}d_T \times[\Delta_R^{(l)}\sin\theta_T\sin\alpha_{RM}^{(w,k)} + \cos\theta_T], \quad (23)$$

$$\epsilon_{w,k,q} \approx R_r^{(k)} - \frac{L_r+1-2q}{2}d_R\cos(\alpha_{RM}^{(w,k)} - \theta_R) \quad (24)$$

where p and q take values from the sets $p \in \{1,\ldots,L_t\}$ and $q \in \{1,\ldots,L_r\}$, respectively, $d_{Tx} = d_T\cos\psi_T\cos\theta_T, d_{Ty} = d_T\cos\psi_T\sin\theta_T, d_{Tz} = d_T\sin\psi_T, d_{Rx} = d_R\cos\psi_R\cos\theta_R$, $d_{Ry} = d_R\cos\psi_R\sin\theta_R, d_{Rz} = d_R\sin\psi_R$.

Finally, the time delays of the multipath components can be inferred from the traversed distances and are given by the following expressions:

$$\tau_{pq}^{LoS} = \frac{\sqrt{D^2+\Delta_H^2}}{c_0}, \quad (25)$$

$$\tau_{m,l}^{SBT} = \frac{D + R_t^{(l)}(1-\cos\alpha_T^{(m,l)})}{c_0\cos\beta_T^{(m,l)}}, \quad (26)$$

$$\tau_{f,l}^{SBT} = \frac{D + R_t^{(l)}(1-\cos\alpha_{TM}^{(f,l)})}{c_0}, \quad (27)$$

$$\tau_{n,k}^{SBR} = \frac{D + R_r^{(k)}(1+\cos\alpha_R^{(n,k)})}{c_0\cos\beta_R^{(n,k)}}, \quad (28)$$

$$\tau_{w,k}^{SBR} = \frac{D + R_r^{(k)}(1+\cos\alpha_R^{(w,k)})}{c_0}, \quad (29)$$

$$\tau_{m,l,n,k}^{DB} = \frac{D}{c_0} + \frac{R_t^{(l)}(1-\cos\alpha_T^{(m,l)})}{c_0\cos\beta_T^{(m,l)}} + \frac{R_r^{(k)}(1+\cos\alpha_R^{(n,k)})}{c_0\cos\beta_R^{(n,k)}} \quad (30)$$

$$\tau_{f,l,n,k}^{DB} = \frac{D}{c_0} + \frac{R_t^{(l)}(1-\cos\alpha_{TM}^{(f,l)})}{c_0} + \frac{R_r^{(k)}(1+\cos\alpha_R^{(n,k)})}{c_0\cos\beta_R^{(n,k)}} \quad (31)$$

$$\tau_{m,l,w,k}^{DB} = \frac{D}{c_0} + \frac{R_t^{(l)}(1-\cos\alpha_T^{(m,l)})}{c_0\cos\beta_T^{(m,l)}} + \frac{R_r^{(k)}(1+\cos\alpha_{RM}^{(w,k)})}{c_0} \quad (32)$$

$$\tau_{f,l,w,k}^{DB} = \frac{D}{c_0} + \frac{R_t^{(l)}(1-\cos\alpha_{TM}^{(f,l)})}{c_0} + \frac{R_r^{(k)}(1+\cos\alpha_{RM}^{(w,k)})}{c_0} \quad (33)$$

where c_0 is the speed of light and $\Delta_H = h_T - h_R$.

III. Space-Doppler Power Spectrum

Assuming a 3-D non-isotropic scattering environment, we have derived the space-time-frequency correlation function (STF-CF) $R_{pq,\tilde{p}\tilde{q}}(\Delta t, \Delta f)$ of the complex faded envelope in (1). Then, we have derived the closed-form expression for the space-Doppler Spectrum of the wideband channel impulse response as the Fourier transform of the space-time-frequency correlation function $R_{pq,\tilde{p}\tilde{q}}(\Delta t, \Delta f)$. The derivations and final expressions are omitted for brevity.

IV. Reference Model Validation

To illustrate validity of the proposed model, we compare the wideband Doppler spectrum with stationary and moving scatterers with the measured Doppler spectrum obtained from the measurement campaign described in [12], the narrowband Doppler spectrum with stationary and moving scatterers in [13], and the narrowband Doppler spectrum with only stationary scatterers in [14].

To verify the proposed reference model with measured data, we need to estimate the model parameters from the measurements. The distance between the $\mathrm{T_x}$ and $\mathrm{R_x}$ (D), the directions and speeds of the $\mathrm{T_x}$ and $\mathrm{R_x}$ (γ_T, γ_R, v_T, and v_R), the azimuth angles of the $\mathrm{T_x}$'s and $\mathrm{R_x}$'s antenna arrays (θ_T and θ_R), the elevation angles of the $\mathrm{T_x}$'s and $\mathrm{R_x}$'s antenna arrays (ψ_T and ψ_R), d_T, d_R, and Δ_H are estimated from the antenna array geometry and the video camera recordings. It is assumed that the path loss exponent γ is 4, which is typical for radio propagation over a flat reflecting surface. The remaining parameters, i.e., the radii R_{t1},R_{r1}, R_{t2},and R_{r2}, the parameters in the von Mises pdfs (k_T, μ_T, k_R, and μ_R), the parameters in the elevation angle pdfs (β_{T_m} and β_{R_m}), the parameters that specify how much the single- and double-bounced rays contribute to the total averaged power (η_T, η_R), the relative velocities of the moving scatterers (v_{TS} and v_{RS}), and the Rice parameter K are estimated from the measured input delay-spread functions. Note that the parameter η_{TR} is equal to $1-\eta_T-\eta_R$ and does not require estimation. To simplify the complexity of the estimator, it is assumed that the moving and stationary scatterers have similar distributions, i.e., $k_T = k_{TM}$, $k_R = k_{RM}$, $\mu_T = \mu_{TM}$, and $\mu_R = \mu_{RM}$. Furthermore, it is assumed that the relative velocities of the scatterers with respect to the $\mathrm{T_x}$ and $\mathrm{R_x}$ are equal, i.e. $v_{TS} = v_{RS}$. Finally, it is assumed the energy contributions from the moving and stationary scatterers are equal, i.e., $\eta_{TS} = \eta_{TM}$, $\eta_{RS} = \eta_{RM}$, and $\eta_{TR1} = \eta_{TR2} = \eta_{TR3} = \eta_{TR4}$. Note that these assumptions are not necessary for the estimator to converge, but are made to speed-up the simulations. Furthermore, we have manually tested different energy distributions between the stationary and moving scatterers and as long as the energy contributed by the moving scatterers is smaller or equal to the energy contributed by the stationary scatterers the statistics were similar.

First, the Rice factor is estimated using the moment-method in [18]. Then, to estimate the parameters $\mathbf{\Theta} = [\beta_{T_m}, k_T = k_{TM}, \mu_T = \mu_{TM}, \beta_{R_m}, k_R = k_{RM}, \mu_R = \mu_{RM}, v_{TS} = v_{RS}, \eta_T, \eta_R]$, we use the maximum likelihood based stochastic

estimator in [12]. The obtained parameters are $\beta_{Tm} = 10.2°$, $\beta_{Rm} = 8.3°$, $\mu_T = \mu_{TM} = 101.4°$, $\mu_R = \mu_{RM} = 281.5°$, $k_T = k_{TM} = 5.5$, $k_R = k_{RM} = 5.2$, $\eta_T = 0.358$, $\eta_R = 0.288$, $\eta_{TR} = 0.354$, $v_{TS} = v_{RS} = 2.35$ m/s, $K = 1.29$, $R_{t1} = R_{r1} = 4.5$ m, and $R_{t2} = R_{r2} = 45$ m.

The channel measurements were collected on the Interstate highway and were performed at 2.435 GHz and the maximum Doppler frequencies of the T_x and R_x were $f_{T\max} = f_{R\max} = 181.72$ Hz (which corresponds to $v_T = v_R = 80.6$km/h). The distance between the T_x and R_x was approximately $D = 180$ m and the moving directions were $\gamma_T = \gamma_R = 90°$. Both, the T_x and R_x were equipped with one omnidirectional antenna with the azimuth and elevation angles $\theta_T = \theta_R = 0°$ and $\psi_T = \psi_R = 0°$, respectively.

Figure 2 compares the proposed wideband Doppler spectrum with stationary and moving scatterers with the measured Doppler spectrum, the narrowband Doppler spectrum with stationary and moving scatterers, and the narrowband Doppler spectrum with only stationary scatterers. The results show that the narrowband Doppler spectrum with only stationary scatterers matches well measured Doppler spectrum for higher Doppler frequencies. However, it does not capture widening of the spectrum around zero frequency. We can observe that the narroband Doppler spectrum with stationary and moving scatterers captures widening of the Doppler spectrum around the zero, but still does not capture all of it. From Fig. 2, we can observe that the wideband Doppler spectrum captures all of the spectrum widening around the zero, and follows well the measured Doppler spectrum toward higher frequencies.

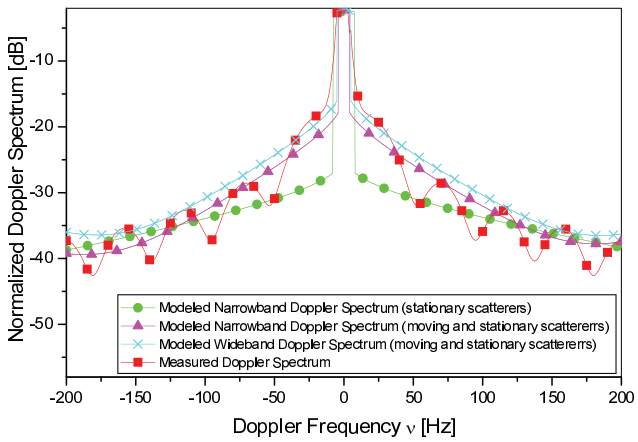

Fig. 2. Theoretical and measured Doppler spectra in an Interstate highway environment.

V. Conclusions

The 3-D geometrical propagation model that includes both stationary and moving scatterers around the transmitter and receiver for wideband V-to-V communications is proposed. Based on the geometrical model, a 3-D reference model for wideband MIMO V-to-V multipath fading channels is developed. From the reference model, the corresponding space-Doppler power spectral density is derived. Finally, the theoretical results are compared with measured data in urban environment, the model with only stationary scatterers, and the narrowband channel model with moving and stationary scatterers. The results show the best agreement between the measured and the modelled wideband propagation model.

References

[1] A. S. Akki and F. Haber, "A statistical model for mobile-to-mobile land communication channel," *IEEE Transactions on Vehicular Technology*, vol. 35, pp. 2–10, Feb. 1986.

[2] C.-X. Wang, X. Cheng, D. I. Laurenson, "Vehicle-to-vehicle channel modeling and measurements: recent advances and future challenges," *IEEE Communications Magazine*, vol. 47, pp. 96–103, Nov. 2009.

[3] A. F. Molisch, F. Tufvesson, J. Karedal, C. .F. Mecklenbrauker, "A survey on vehicle-to-vehicle propagation channels," *IEEE Transactions on Wireless Communications*, vol. 16, pp. 12–22, Dec. 2009.

[4] V. H. Pham, M. H. Taieb, J. Y. Chouinard, S. Roy, and H. T. Huynh, "On the double Doppler effect generated by scatterer motion," *REV Journal on Electronics and Communications*, vol. 1, pp. 30–37, Mar. 2011.

[5] S. Roy, H. T. Huynh, and P. Fortier, "Compound Doppler spread effects of subscriber motion and scatterer motion," *International Journal of Electronics and Communications*, vol. 57, pp. 237–246, Jan. 2003.

[6] S. Thoen, L. Van der Perre, M. Engels, "Modeling the channel time-variance for fixed wireless communications," *IEEE Communications Letters*, vol. 6, pp. 331–333, Aug. 2002.

[7] A. Domazetovic, L. J. Greenstein, N. B. Mandayam, and I. Seskar, "Estimating the Doppler spectrum of a short-range fixed wireless channel," *IEEE Communications Letters*, vol. 7, pp. 227–229, May 2003.

[8] J. B. Andersen, J. O. Nielsen, G. F.Pedersen, G. Bauch, and G. Dietl, "Doppler spectrum from moving scatterers in a random environment," *IEEE Transactions on Wireless Communications*, vol. 8, pp. 3270–3277, June 2009.

[9] A. Borhani and M. Pätzold , "Modeling of vehicle-to-vehicle channels in the presence of moving scatterers," *Proceedings of IEEE Vehicular Technology Conference VTC Fall'12*, pp. 1–5, Quebec City, Canada, Sept. 2012.

[10] A. Chelli and M. Pätzold, "A Non-stationary MIMO vehicle-to-vehicle channel model derived from the geometrical street model," *Proceedings of IEEE Vehicular Technology Conference VTC Fall'11*, pp. 1–6, San Francisco, CA, Sept. 2011.

[11] A. Chelli and M. Pätzold, "The impact of fixed and moving scatterers on the statistics of MIMO vehicle-to-vehicle channels," *Proceedings of IEEE Vehicular Technology Conference VTC Spring'09*, pp. 1–6, Barcelona, Spain, April 2009.

[12] A. Zajić, G. Stüber, T. Pratt, S. Nguyen, "Wideband MIMO mobile-to-mobile channels: geometry-based statistical modeling with experimental verification," *IEEE Transactions on Vehicular Technology*, vol. 58, pp. 517–534, Feb. 2009.

[13] A. Zajić,"Impact of moving scatterers on vehicle-to-vehicle narrowband channel characteristics," *IEEE Transactions on Vehicular Technology*, vol. 63, pp. 3094–3106, Sept. 2014.

[14] A. G. Zajić and G. L. Stüber, "Three-dimensional modeling, simulation, and capacity analysis of spacetime correlated mobile-to-mobile channels," *IEEE Transactions on Vehicular Technology*, vol. 57, pp. 2042–2054, July 2008.

[15] D. Gesbert, H. Bölcskei, D.A. Gore, and A.J. Paulraj, "Outdoor MIMO wireless channels: models and performance prediction," *IEEE Trans. on Commun.*, vol. 50, pp. 1926–1934, Dec. 2002.

[16] A. Abdi, J. Barger, and M. Kaveh, "A parametric model for the distribution of the angle of arrival and the associated correlation function and power spectrum at the mobile station," *IEEE Trans. on Veh. Tech.*, vol. 51, pp. 425–434, May 2002.

[17] J.D. Parsons and A.M.D. Turkmani, "Characterisation of mobile radio signals: model description," *IEE Proc. I, Commun., Speach, and Vision*, vol. 138, pp. 549–556, December 1991.

[18] L. J. Greenstein, D. G. Michelson, and V. Erceg, "Moment-method estimation of the Ricean K-factor," *IEEE Commun. Letters*, vol. 3, pp. 175–176, June 1999.